Nat. Hazards Earth Syst. Sci., 14, 831–848, 2014
www.nat-hazards-earth-syst-sci.net/14/831/2014/
doi:10.5194/nhess-14-831-2014

Natural Hazards and Earth System Sciences
Open Access

Integrating geomechanical surveys and remote sensing for sea cliff slope stability analysis: the Mt. Pucci case study (Italy)

S. Martino and P. Mazzanti

Department of Earth Sciences and CERI Research Centre, University of Rome "Sapienza", P. le Aldo Moro no. 5, 00175, Rome, Italy

Correspondence to: P. Mazzanti (paolo.mazzanti@uniroma1.it)

Received: 28 June 2013 – Published in Nat. Hazards Earth Syst. Sci. Discuss.: 31 July 2013
Revised: 20 February 2014 – Accepted: 23 February 2014 – Published: 11 April 2014

Abstract. An integrated approach to the geomechanical characterization of coastal sea cliffs was applied at Mt. Pucci (Gargano promontory, Southern Italy) by performing field-based geomechanical investigations and remote geostructural investigations via a terrestrial laser scanner (TLS). The consistency of the integrated techniques allowed to achieve a comprehensive and affordable characterization of the main joint sets on the sea cliff slope. The observed joint sets were considered to evaluate the proneness of the slope to rock failures by attributing safety factor (SF) values to the topple- and wedge-prone rock blocks under three combined or independent triggering conditions: (a) hydrostatic water pressures within the joints, (b) seismic action, and (c) strength reduction due to weathering of the joint surfaces. The combined action of weathering and water pressures within the joints was also considered, resulting in a significant decrease in the stability. Furthermore, remote survey analyses via InfraRed Thermography (IRT) and Ground Based Synthetic Aperture Radar Interferometry (GBInSAR) were performed to evaluate the role of the surveyed joint sets in inducing instabilities in the Mt. Pucci sea cliff. The results from the remote surveys: (i) GBInSAR monitoring revealed permanent displacements coupled to cyclic daily displacements, these last ones detected in certain sectors of the cliff wall; (ii) the thermal images allowed us to identify anomalies that correspond well to the main joints and to the slope material released due to recent collapses.

1 Introduction

Due to the rapid development of coastal settlements and the increasing population located in coastal regions, substantial efforts are required to manage the possible risks associated with natural hazards in these areas (Pennetta and Russo, 2011; Montoya-Montes et al., 2012; Dewez et al., 2013; Epifanio et al., 2013; Marques et al., 2013; Stanchev et al., 2013). It is estimated that more than 37 % of the world's population live within 100 km of the coastline and that 80 % of these shores are rocky (Emery and Kuhn, 1982). In addition to coastal settlements, rapid landslides can be particularly dangerous for near-shore structures and infrastructure, such as oil platforms and submarine pipelines. These structures can be severely damaged by coastal landslides in both the detachment areas and the regions affected during propagation (e.g., Heezen and Ewing, 1952; Assier-Rzadkiewicz et al., 2000; Bozzano et al., 2011a; L'Heureux et al., 2011; Schulz et al., 2012; Force, 2013).

Although they are not the most dangerous events, rockfalls, topples, and large collapses from sea cliffs are the most common slope instabilities in coastal regions. These events commonly involve small volumes (e.g., single blocks), but they may involve larger sizes, thus significantly increasing the risk to near-shore settlements and activities (Hampton et al., 2004).

Furthermore, rockfalls are a fundamental component of landscape evolution in rocky coasts, contributing to a high erosion rate, which can reach several decimeters per year (Duperret, 2002, 2004; Mortimore, 2004; Lim et al., 2009; Santos et al., 2011; Katz and Mushkin, 2013).

Rockfalls are a widespread problem on high coastal cliffs, and in certain regions, these cliffs represent a large percentage of the total coast. For example, 15 % of Italian coasts are rock cliffs. Furthermore, the prediction of coastal rockfalls is quite complex, and physical investigation is the most common approach for hazard assessment purposes.

Moreover, coastal landslides can be responsible for induced hazards such as in the case of tsunamis, as demonstrated by several recent events (e.g., Assier-Rzadkiewicz et al., 2000; Tappin et al., 2001; Papadopoulos and Kortekaas, 2003; Tinti et al., 2004; Mazzanti and Bozzano, 2011; Bregoli et al., 2013). In such a contest, monitoring systems should be designed and adapted in terms of the following specific requirements: (i) to investigate or detect cliff slopes at different evolutionary stages (forward prevention), i.e., corresponding to different distributions the landslide hazard; (ii) to understand and control the parameters for forecasting the short-term evolution of gravitational instabilities (such as high-velocity landslides) and for the planning of alert systems (real-time prevention).

This paper reports the results of a detailed investigation carried out on a 45 m-high sea cliff for the assessment of its overall stability by examining different triggering processes. The sea cliff, located in the Gargano National Reserve (Southern Italy), is composed of fractured and weathered limestones and chalks and is frequently affected by rockfalls. Direct traditional geomechanical field surveys and remote laser scanner surveys were performed. More in particular, data collected from traditional field surveys in the surroundings of the inaccessible cliff were integrated with pervasive joint set characterization using a terrestrial laser scanner (TLS)-derived high-resolution point cloud as extensively presented in the scientific literature (e.g., Sturzenegger and Stead, 2009; Oppikofer et al., 2009).

In addition, short GBInSAR and InfraRed Thermographic (IRT) surveys were performed, thus trying to detect micromovements of localized blocks and a preliminary assessment of the rock mass thermal features, respectively.

The experienced investigations stimulate a discussion on how the combination of traditional and laser scanner surveys applied to sea cliffs can be integrated to provide more accurate and complete information, due to the peculiarities of the considered slopes.

2 Sea cliff investigation and landslide hazards

Among coastal slopes, high cliffs are of particular interest in terms of risk mitigation because of their complex evolution that involves the coupled action of marine erosion and gravity-induced slope instability (Hampton et al., 2004; Dickson et al., 2013; Della Seta et al., 2013; Mantovani et al., 2013). In this regard, coastal hazards will probably be one of the major topics for society regarding natural risk management in this century for different reasons, including: the sea level rise, the effects on the inland river remove and the increasing anthropic pressure. This last feature is causing an increasing density of population distributed in the coastal regions and consequently an increasing exposure to natural risks (Mc Chulloug et al., 2013), as proved by the recent disasters caused at the Maldives Islands and the Japan Honshu coasts by the 2004 and 2011 tsunamis, respectively, and at the Philippine Islands by the 2013 Hayan typhoon.

The high rate of occurrence of slope failures affecting costal cliffs is hazardous not only because of the direct effect of the falling masses but also as a result of induced effects, such as tsunamis (resulting from falls in the sea), shock wave propagation (resulting from falls on the shore), and the development of new fractures along the cliff edge.

To reduce the risk associated with these phenomena, advanced and multi-parameter techniques are now available for monitoring cliffs subject to erosion and sudden collapse. This approach requires the integration of geophysical and geological investigations to foresee a potential slope failure and to provide civil protection agencies with an effective tool to alert and secure people and structures exposed to the event.

Because of the morphology and height of coastal cliffs and their complex visibility, the installation of remote monitoring devices (e.g., TLS, GBInSAR, IRT) requires specialized technical implementation.

Field mapping of rock discontinuities is the most common approach for the analysis of rock cliffs. This classical geomechanical investigation allows the main joints to be characterized in terms of dip, dip direction, widening, the presence of gouge material, persistency, and other factors (see Hatheway, 2009 for a comprehensive review). Furthermore, the mechanical features of the rock mass, including the surface roughness and the rock compressive strength, can be assessed with field instruments and laboratory experiments. Nevertheless, high coastal cliffs are difficult to access directly and, therefore, cannot be easily and comprehensively investigated using traditional field methods (Cheryl and Hapke, 2004; De Vita et al., 2012), resulting in high costs or, more often, low information density.

Cliff slope evolution is strongly conditioned by the geological setting and by the jointing conditions of the involved rock masses. Surveying these features and inventorying the slope instabilities enables the performance of statistically based analyses of the susceptibility of sea cliffs to rockfalls (Lee et al., 2001, 2002; Lim et al., 2010; Marques et al., 2011, 2013). In addition to the most common preconditioning and triggering factors that control rockfalls from inland cliffs (e.g., rainfall, earthquakes, cyclic temperature variations, plant root growth), further factors must be considered for coastal cliffs. For example, tidal variations, basal erosion induced by waves, and sea storms induce additional stresses on the rock mass (Senfaute et al., 2009; Violante, 2009; Katz and Mushkin, 2013, and references therein).

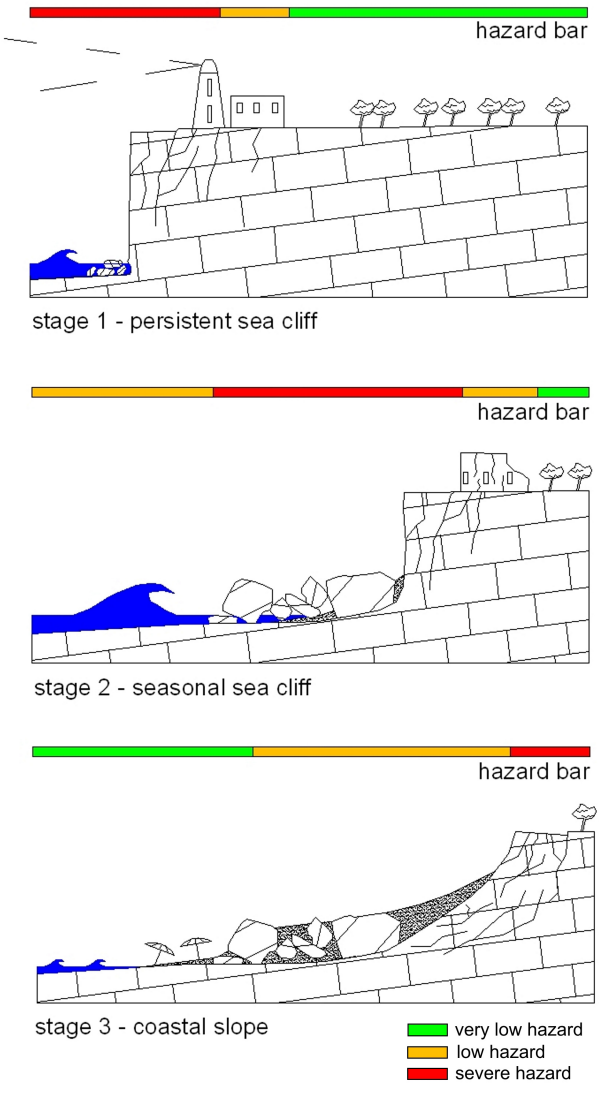

Fig. 1. Conceptual model showing the evolution from a sea cliff to a cliff slope and the related hazard levels.

A basic conceptual model of the evolution of a sea cliff toward a coastal slope can be summarized in the following three steps (Fig. 1):

1. "Persistent sea cliff": A sea cliff evolves via progressive retreat as an effect of shoreline erosion due to sea waves. In this stage, the slope instabilities are primarily represented by rockfalls and toppling, i.e., gravitational instabilities characterized by impulsive and recurrent events.

2. "Seasonal sea cliff": The sea cliff is seasonally involved in marine erosion only as an effect of the strongest sea storms, and a talus deposit is formed during the non-storm periods.

3. "Coastal slope": The sea cliff is definitively abandoned by the sea, no marine erosion occurs except during exceptional storm events, a beach is formed that separates the old cliff from the present shoreline, and the slope retreat of the coastal slope is primarily due to sliding mechanisms, which cause a progressive decrease in the slope angle.

The model of the sea cliff evolution described above corresponds to a gradual reduction in the natural risks of the coastal area (Marques, 2008 and references therein).

With reference to the above-listed stages, it is possible to associate the "persistent cliff slope stage" with a natural risk consisting of impulsive rockfall events that affect the adjacent pocket beaches and, in the case of large volumes, induce tsunami waves. In addition, the instantaneous retreat of the cliff can drastically affect structures or buildings located along the sea cliff border.

In the "seasonal cliff slope stage", the natural risk is related to impulsive events that can affect an emerged beach, i.e., during the non-storm period, and they constitute a potential hazard for visitors.

Finally, the "coastal slope stage" corresponds to a minor risk for visitors because the landslide mechanisms are different. Typical preconditioning and triggering factors related to the sea action are no longer effective; hence, the instabilities are less abrupt. However, in this stage, larger landslides may occur, leading to major risks for structures or infrastructure located near the top of the cliff slope.

The evolution of a sea cliff toward a costal slope predisposes it to different landslide mechanisms (Hutchinson, 1988, 1991). In the "persistent sea cliff stage", the cliff retreat is characterized by stiff outcropping rocks characterized by high-angle primary joint sets. The progressive retreat and the resulting stress release cause the generation of secondary joint sets that are nearly parallel to the slope face and whose openings generally increase with decreasing distance from the cliff; these joints contribute to failures of the slope face, such as falls and topples. In the "seasonal sea cliff stage," the average rate of retreat decreases and the longer exposure of the cliff causes the weathering processes to occur more pervasively, predisposing the cliff to more intense instabilities during storms. Finally, in the "coastal slope stage", the secondary joint sets are not necessarily located parallel to the slope face, and intense weathering processes can occur that favor landslide triggers and control the strain rate of the sliding processes.

3 Study area: Mt. Pucci sea cliff (Gargano promontory, Italy)

The Gargano promontory is located in Southern Italy and its coastline is of particular interest from a naturalistic point of view, as it is part of a national park (instituted in 1991) about

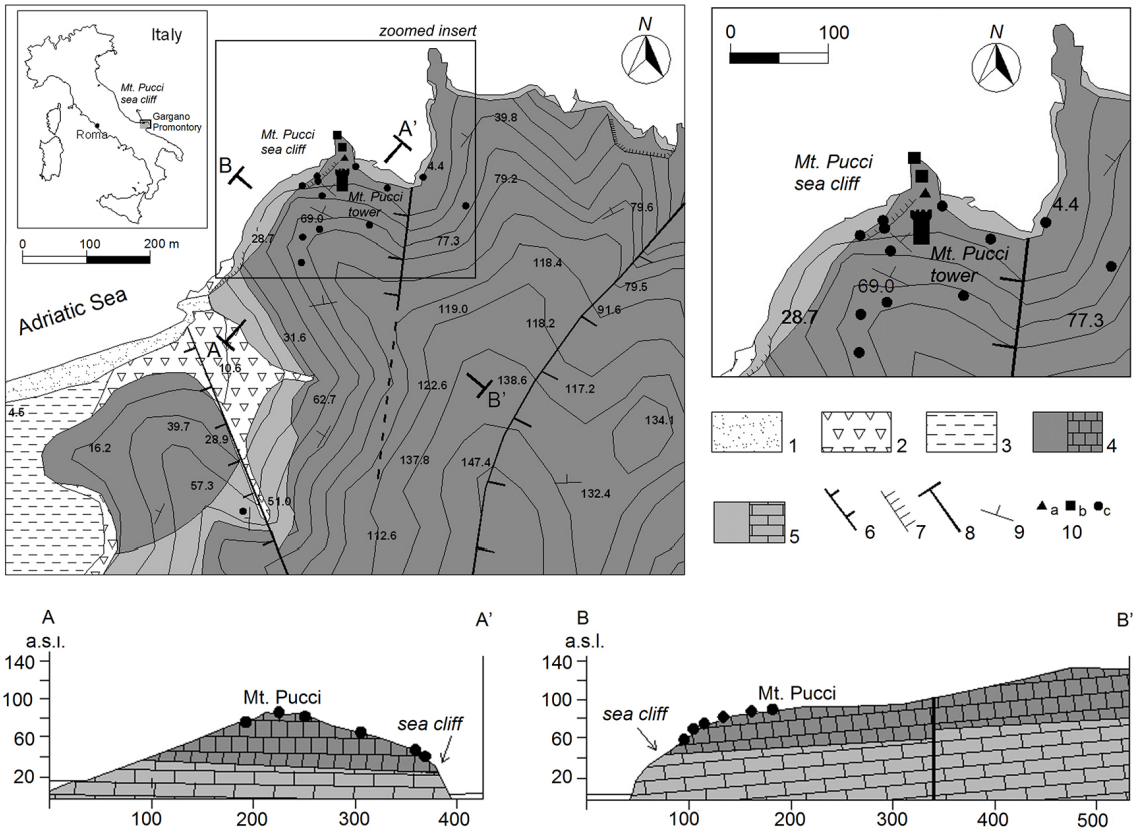

Fig. 2. Geological sketch of the Mt. Pucci coastal area: (1) coastal deposits; (2) slope debris; (3) alluvia; (4) calcarenites of the Peschici Fm. (PSH), Eocene; (5) marly limestones of the Scaglia Fm. (SC), lower–middle Cretaceous; (6) certain fault; (7) cliff scarp; (8) trace of geological section; (9) attitude of beds; (10) measurement points: **(a)** GBInSAR, **(b)** TLS and IRT, **(c)** geomechanical scanlines.

121 000 ha in extent and which hosts several villages (including Peschici and Vieste among others) that are part of the cultural and touristic heritage of the Apulia region. The Gargano promontory is characterized by almost 150 km of coastline corresponding to sea cliffs for several tens of kilometers.

The Mt. Pucci sea cliff is located on the northern side of the Gargano promontory, close to the village of Peschici. Mt. Pucci exhibits a hill-type relief with a maximum elevation of approximately 150 m a.s.l. (Fig. 2). According to the wavemeter records, the most frequent sea storms in the Gargano promontory originate from the northeast, and the height of the strongest waves reaches 4 m, with a frequency of 10–25 %. Notably strong storms are only rarely recorded from the north, with a maximum wave height of 5.2 m (ISPRA, 2012).

The Gargano promontory is a portion of the carbonatic Apulia Platform that represents one of the most important paleogeographic units of the middle–southern Italian Apennines (Bosellini et al., 1999). This paleogeographic unit was formed during the Mesozoic (from the lower Jurassic up to the middle Cretaceous period) in Bahamas-like conditions, and it currently represents the most external domain of the Apennine Chain in the southern Adriatic area. According to Bosellini and Morsilli (1997), beginning in the middle–upper Cretaceous and throughout the Paleocene, the Apulia Platform was gradually destroyed due to the combined effects of eustatism (also responsible for many Paleocene emersion phases), tectonic uplift, and strong earthquakes. This destruction is evidenced by megabreccia deposits (Grottone deposits) and bioclastic turbidites (Peschici Fm.), which crop out widely in the Gargano area (Bosellini and Morsilli, 1997).

The Gargano promontory area is characterized by EW-oriented tectonic elements corresponding to transform fault lines (Billi and Salvini, 2000) and, in particular, it constitutes a horst involved in a wide anticline fold system with a WNW–ESE-oriented axis. This anticline structure is crossed by numerous left transtensive faults, with orientations varying from E–W to NW–SE. These faults are primarily concentrated in the southern portion of the area, corresponding to the anticline hinge. Among these elements, the Mattinata fault represents the main regional structure related to an evident local geomorphological landform (Billi and Salvini, 2000) and to many seismogenetic sources capable of earthquakes up to 6.4 M_w (DISS3.1, 2010) that are expected with a recurrence interval from several hundred to several

Fig. 3. Photo view of the Mt. Pucci cliff slope. View is to the east (see Fig. 2 for the location of the measurement points). From this location, some remote sensing-based surveys (TLS and IRT) were conducted.

thousand years. Based on the CEDIT catalogue (Fortunato et al., 2012), any earthquake-induced effects have been historically documented on the northern coast of the Gargano promontory. According to Bosellini and Morsilli (2001) and based on surveys filed by the same authors, the following geological formations crop out in the Mt. Pucci area:

- Maiolica (MA) Fm. (lower Cretaceous): micritic white limestone with chert, mildly to thinly layered;
- Scisti a Fucoidi (SF) Fm. (lower Cretaceous): white micritic limestone and gray marly limestone, mildly to thinly layered;
- Scaglia (SC) Fm. (lower–middle Cretaceous): white marly limestone with brown chert, mildly to thinly layered;
- Peschici (PSH) Fm. (Eocene): white bioclastic calcarenite with nummulites and echinids, mildly to thickly layered.

In particular, the PSH and the SC Fm.s crop out on the Mt. Pucci sea cliff with a 30/10 (dip direction/dip) attitude in the strata.

Field evidence reveals that the Mt. Pucci coastal cliff is widely involved in rockslides responsible for a clearly visible talus at the bottom of the slope (Fig. 3). The main predisposing conditions for these instabilities are the subvertical face of the cliff and the intense erosion processes due to the sea, which continuously excavate the base of the cliff. Moreover, the visible weathering processes can be primarily related to intense thermal variation (both diurnal and seasonal) due to the north-facing aspect of the cliff as well as to the nebulized salt water from the sea waves.

The annual average rainfall measured at Vico del Gargano (close to Peschici) is 810 mm yr^{-1}, with an average annual temperature of approximately 15 °C (Polemio et al., 2000).

4 Geomechanical analysis and terrestrial laser scanner survey

Based on the previously reported model of the evolution of a cliff slope toward a coastal slope, Mt. Pucci represents a persistent sea cliff, corresponding to the first stage of the above-depicted evolution model. The geomechanical investigations in this study were focused on the reconstruction of the rock mass joint setting because it represents a fundamental feature that defines the failure model for the sea cliff during the initial stage, and on the evaluation of landslide susceptibility and the stability conditions of the slope.

4.1 Direct geomechanical survey

The geomechanical characterization of the calcarenites and the marly limestones that crop out on the Mt. Pucci coastal cliff slope (ascribable to the PSH and SC Fm.s, respectively) was carried out via a traditional geomechanical survey performed according to the ISRM (2007) standard. This survey was focused on evaluating and dimensioning both the rock mass jointing conditions and the strength properties. To this aim, the main joint sets of the rock masses together with their attitude, geomechanical properties (i.e., spacing, opening, jointing conditions, standard joint indexes J_v and I_b – ISRM, 1978, 2007) were measured as well as strength parameter values by using a Schmidt Hammer sclerometer and a Barton Comb. profilometer.

Due to the reduced accessibility of the cliff slope, 11 geomechanical scanlines were performed on the surrounding cliff area (Fig. 2), including nine on the PSH calcarenites and two on the SC marly limestones. Four other geomechanical survey stations were directly carried out by climbers on the wall of the coastal cliff slope where the PSH calcarenites crop out.

The poles of the measured joints were plotted using the "RockScience Dips – free demo version" code from the Schmidt equi-areal stereographic projection (lower hemisphere). The attitudes of the main joint sets were deduced, as suggested by ISRM (1978), using Fisher concentration contour lines and attributing a joint set attitude if the concentration value was greater than 5 %. Following this approach, five main joint sets (J1 to J5) were recognized in the PSH calcarenites, and only two main joint sets were recognized in the SC marly limestones (see Table 1 for the joint set parameters). For both the PSH and the SC rock masses, the J1 set corresponds to stratification.

The strength parameter values of the joint sets were attributed according to the Barton and Bandis (1973, 1990) failure criterion. To this aim, the joint roughness coefficient

Table 1. Joint parameters from the field-based geomechanical surveys.

Lithology	Joint set	Dip direction azimuth	Dip (°)	Spacing (cm)	Jv (joint m^{-3})	Ib (cm)
PSH	J1 (strata)	24	11	59		
PSH	J2	247	65	40	8	69
PSH	J3	270	87	36		
PSH	J4	301	87	62		
PSH	J5	360	81	53		
SC	J1 (strata)	23	16	24	12.5	25
SC	J2	258	68	21		

Table 2. Physical and mechanical properties of the intact PSH and SC rock based on laboratory tests. γ_s – solid weight of unit volume; γ_n – weight of unit volume; $I_{s(50)}$ point load index (ASTM D5731-08), $q_{c(20-25\%Is(50))}$ point load strength (ASTM D5731-08).

Lithology	γ_s (kN m^{-3})	γ_n (kN m^{-3})	$I_{s(50)}$ (MPa)	$q_{c\,(20–25\%\,I_s\,50)}$ (MPa)
PSH	26.80	23.44	3.11	62.11–77.63
SC	26.86	23.23	3.18	63.51–79.38

(JRC) and the joint compressive strength (JCS) of the main joint sets were measured and the values of the intact rock friction angle (φ_b) were attributed on the basis of literature data sets (De Vallejo, 2005). To select the most appropriate φ_b value the UCS strength values specifically measured in the Laboratory of Engineering Geology of the Sapienza University of Rome from point load tests were used (ASTM D5731-08 and ISRM, 1977; 1985 standards) (Table 2) .

4.2 Remote measurements: laser scanner surveys

Remote geomechanical surveys were performed using a laser scanner integrated with a high-resolution digital camera and supported by a D-GPS survey.

Surveys were performed on 12 November 2010, using a Riegl VZ400 laser scanner combined with a Nikon D700 camera with a 14 mm lens and a luminosity of 1.2 and one GPS-Glonass unit (model Topcon Hyper Pro).

Laser scanner data were collected from two different scan positions to reduce the shadow zones and to obtain mm-scale accuracy of the detected points (Fig. 4). Nevertheless, due to the difficult accessibility of the cliff and the unfavorable exposure of the cliff face, it was not possible to achieve a "shadow-free" point cloud. Optical markers were applied all around the surveyed area to align the data collected from the two scan positions and to translate the detected coordinates to the UTM-WGS84 coordinate system via the built-in GPS sensor (Fig. 4). RGB colors of the detected points were collected by using a Nikon D700 digital camera integrated with the VZ400 sensor. Hence, a true-color point cloud of the cliff

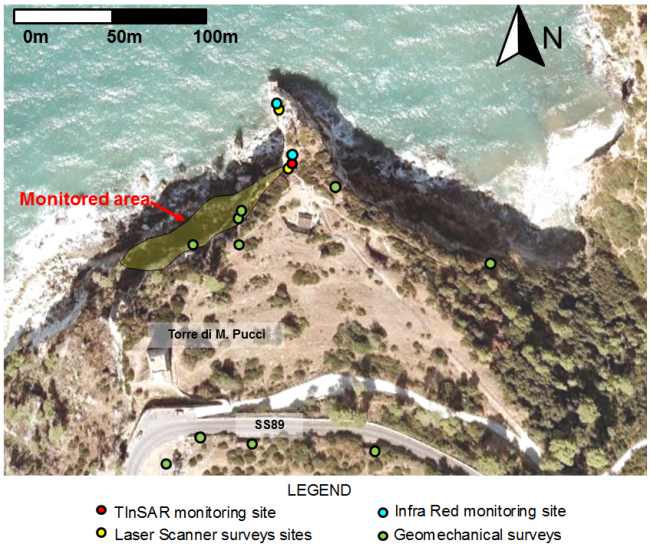

Fig. 4. Aerial photo of the Mt. Pucci area showing the investigated sector (Mt. Pucci Cliff); the locations of the GBInSAR, TLS, and IRT remote surveys; and the geomechanical stations.

consisting of approximately 45 million points with a density of approximately 1 point/cm was derived (Fig. 5).

Both manual and automatic analyses of the point cloud were performed to derive information on the joint pattern features. The AdHoc3D software (http://www.adhoc3d.com/en/adhoc/) was used for the manual analysis, which was performed by two researchers to reduce the subjectivity in the identification of joints. Specifically, joint surface orientation was derived by manual selection of the operator of at least three points visually recognized as being located on the same joint surface.

Automatic analysis was performed using both the Split-FX-Free Demo Version (http://www.spliteng.com/split-fx/) and the Coltop3D-Free Demo version (Jaboyedoff et al., 2007) software (Fig. 6). Using the Split-FX software, the automatic analysis identified enough points to depict a surface whose attitude in space can be measured. The automatic surface identification was based on a user-defined threshold

Table 3. Joint parameters from the remote measurements.

Lithology	Joint set	Dip direction azimuth	Dip (°)	Spacing (cm)	Jv (joint m^{-3})	Ib (cm)
PSH	J1 (strata)	20	15	64		
PSH	J2	253	75	39	3.2	54
PSH	J3	300	82	59		
PSH	J4	350	87	54		
SC	J1 (strata)	28	10	21	9.7	44
SC	J2	120	82	67		

Table 4. Geomechanical properties attributed to the recognized joint sets: JRC – joint roughness coefficient, JCS – joint compressive strength (Barton and Bandis, 1973, 1990), σ_n – normal stress acting on the joints, φ_b – intact rock fiction angle, φ_p – joint friction angle, φ_p – residual joint friction angle, r/R – weathering joint ratio, φ_p – weathered friction angle (De Vallejo, 2005).

Lithology	Joint set	Dip direction azimuth	Dip (°)	Spacing (cm)	JCS (MPa)	JRC	σ_n (kPa)	ϕ_b (°)	ϕ_p (°)	r/R	ϕ_r (°)	ϕ_{wth} (°)
PSH	J1 (strata)	21	15	64	64	10	129	34	31	0.2	18	15
PSH	J2	300	88	59	46	12	129	34	29	0.4	22	17
PSH	J3	358	90	54	45	17	129	34	26	0.6	26	18
PSH	J4	269	87	34	44	14	129	34	27	0.8	30	23
PSH	J5	253	70	39	44	18	129	34	26	1	34	26
SC	J1 (strata)	25	10	21	40	14	128	31	24	nd	nd	nd
SC	J2	300	80	67	42	12	128	31	25	nd	nd	nd

Fig. 5. TLS point cloud of the Mt. Pucci cliff colored by the optical photos.

value of points that must all lie in the same plane. Specifically, both supervised (i.e., patches selected by the operator) and unsupervised analysis was performed and the results were then combined. Such an approach allowed us to perform detailed analyses of the entire outcropping cliff (by analyzing a large amount of surfaces in a few minutes) and represents an objective analysis. Furthermore, thanks to the high-density point cloud, information on small surfaces was derived. However, certain weaknesses in performing an "automatic analysis" must be accounted for. First, not all exposed surfaces can be identified, depending on their orientation with respect to the TLS point of view. Second, the sizes of the exposed surfaces used for the automatic recognition are crucial and their selection requires skilled evaluation by the operator. Moreover, the Mt. Pucci data were collected only on the eastern side of the cliff (Fig. 4), and hence the rock joints with an approximately westerly dip direction cannot be identified.

However, "manual analysis" allowed us to avoid certain limitations that affect the "automatic analysis", enabling us to characterize the stratification joint set in detail.

Table 3 summarizes the main joint sets and their average spacing values derived from the remote measurements for the PSH and the SC Fm.s. Two main joint sets were identified in the SC Fm., and four main joint sets were detected in the PSH Fm.

All the available data, from both manual and TLS surveys, were used for computation of the J_v parameter (Palmstrom 1982, 1985, 1986, 1996; Sen and Eissa, 1992). J_v values of 3.2 and 9.7 were estimated for the PSH Fm. and the SC Fm., respectively (Table 3).

Figure 7 displays the final stereo plots derived from the combined automatic and manual analysis of the TLS point cloud for the PSH Fm. and SC Fm., respectively. Table 4

Table 5. Joint combinations and related rock block geometries compatible with topples at the Mt. Pucci cliff slope.

Slope face (dip dir/dip)	Basal joint (dip dir/dip)	Lateral joint_1 (dip dir/dip)	Lateral joint_2 (dip dir/dip)	Spacing_1 (m)	Spacing_2 (m)	H (m)	b (m)	ψ (°)	ϕ (°)
355/80	21/15	300/88	358/90	0.59	0.55	0.64	0.55	15	31
355/80	21/15	300/88	253/70	0.59	0.39	0.64	0.48	15	31
355/80	21/15	300/88	269/87	0.59	0.34	0.64	0.5	15	31
355/80	21/15	358/90	269/87	0.54	0.34	0.64	0.64	15	31
355/80	21/15	358/90	253/70	0.54	0.39	0.64	0.64	15	31
355/80	21/15	269/87	253/70	0.34	0.39	0.65	0.38	15	31

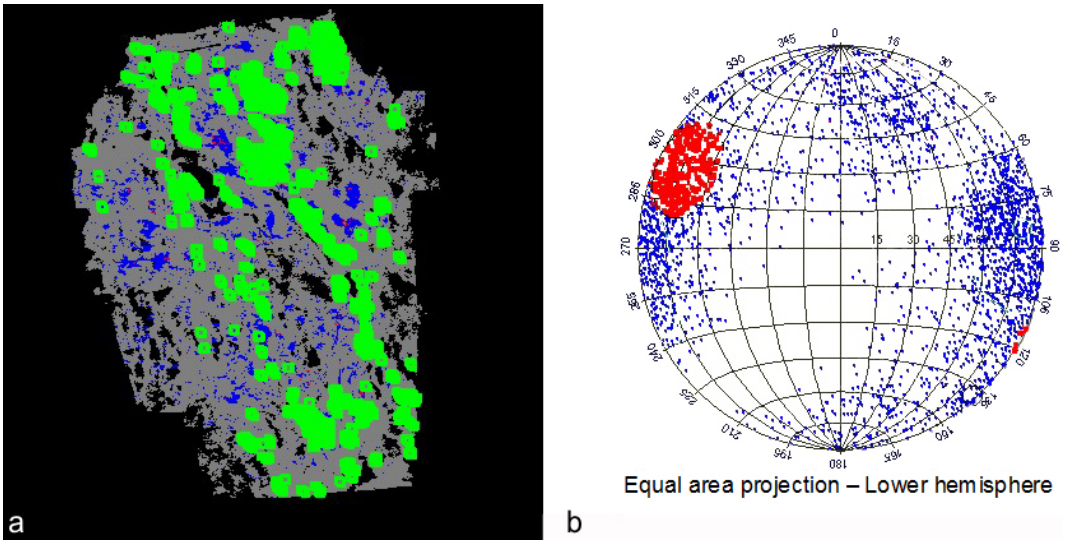

Fig. 6. Sketch showing the results of the automatic detection of the main joint sets from a laser scanner-georeferenced points cloud; **(a)** points cloud of a portion of the cliff (grey color) with the automatic identification of planes (blue color) and selection of some planes of the same joint set (green dots); **(b)** stereo plot showing the poles of the planes automatically detected (blue dots) on the points cloud and poles selected in the side image (red dots).

summarizes the geomechanical parameters attributed to all the distinguished joint sets.

5 Stability conditions of the Mt. Pucci sea cliff

5.1 Proneness to rock failures

The stability conditions of the Mt. Pucci sea cliff were analyzed by taking into account the results of the geomechanical surveys performed on the rock mass that crops out on the slope face. The primary (strata) and secondary (fractures) joint sets on the Mt. Pucci sea cliff play a fundamental role in controlling the slope instabilities.

Three failure mechanisms were therefore considered for the slope stability analysis (Duncan and Christopher, 2004) by taking into account the attitude of the main measured joint sets: (1) rock plane sliding, (2) rock topples, and (3) rock wedge slides.

For each considered failure mechanism, a preliminary kinematic analysis was performed using the Markland (1972) tests for both slides and topples. The tests were performed by considering all of the possible combinations of joint sets and identifying those capable of meeting the established kinematic criteria. Moreover, to perform a more detailed kinematic analysis, four slope face orientations (dip direction/dip) were considered (355/80, 320/75, 345/70, and 300/60, as measured from east to west along the cliff wall). This selection was based on the point cloud provided by the laser scanner survey in addition to the average orientation of the sea cliff slopes (330/70).

The stability analysis was performed for these combinations of joint sets to attribute a safety factor (SF) under different destabilizing conditions. The analytic solutions were mathematically computed except for the rock wedge sliding, which was analyzed using the "Wedge Failure Analysis Version 2.0 free version" code.

The Markland tests provided the following outputs:

1. Kinematic compatibility with rock topples exists only in the case of the 355/80-oriented slope face by combining the sub-horizontal stratification set J1 with the sub-vertical joint set J3 of Table 4 and by considering

all combinations with the other sets (J2, J4, J5) as lateral joints;

2. Kinematic compatibility with rock wedge sliding exists for all of the slope face orientations except for the PSH calcarenites alone and the combinations of joint sets reported in Table 5;

3. No kinematic compatibility exists with sliding rock failures.

5.2 Stability analyses

The stability conditions of the Mt. Pucci sea cliff were tested for rock topples and rock wedge sliding because these two mechanisms showed kinematic compatibility based on the Markland tests.

The stability analyses were performed under static and pseudo-static conditions (i.e., considering seismic action). In addition, possible destabilizing factors were taken into account, such as static water pressure within the joint sets and weathering of the joints (the latter was applied to the rock wedge sliding mechanism only).

In the case of rock topples, considering the joint properties summarized in Table 4, the stability chart of Fig. 8 (Goodman and Bray, 1977) demonstrates that stable conditions can be expected for the coastal cliff wall of Mt. Pucci under static conditions and without external actions (i.e., water pressures within opened joints or seismic forces).

Based on these equilibrium conditions, the static level of the water filling the subvertical set J3 should reach approximately 50 cm before causing block topples.

Moreover, if a pseudo-static acceleration k_x is applied to the blocks, i.e., the weight force is deflected downslope, the critical pseudo-static acceleration k_{cr} required to reach disequilibrium condition, and could cause block topples.

Based on the Goodman and Bray (1977) assumptions by simply taking into account a horizontal pseudostatic action (see the chart in Fig. 8), under static condition, the topple on an inclined plane occurs if

$$(b/h = \tan\beta) < \tan\psi, \tag{1}$$

where b/h is the geometrical ratio of the rock block (i.e., b is the length and h is the height), and ψ is the dip angle of the basal plane. To report the equilibrium under critical conditions for a horizontal pseudostatic action we have to assume that

$$(\tan\beta + \tan\Delta\alpha) = \tan\psi, \tag{2}$$

where $\tan\Delta\alpha = k_{cr}$. So, it is possible to derive that

$$\tan\Delta\alpha = |tan\psi - \tan\beta| = k_{cr}. \tag{3}$$

According to Eq. (3), the average critical pseudo-static acceleration (k_{cr}) for triggering rock topples is equal to 0.25 g, which corresponds to a recurrence interval of approximately 1000 years for the Mt. Pucci area (INGV, 2006).

In the case of rock wedge sliding, the stability analysis was performed using the "Wedge Failure Analysis Version 2.0 free version" code and adopting the approach of Hoek and Bray (1981). The wedge geometries were hypothesized by combining the five individuated joint sets; the presence of tension cracks only results in the 335/80 slope face orientation when considering the 358/90 joint set. The wedge dimensions are automatically computed by the software and considered for quantifying the inertial forces for evaluating the SF.

Because no rock wedges resulted for the SC marly limestones, the stability analysis was performed only for the PSH calcarenites. The results from the data reported in Table 5 show that stable conditions were found for all of the hypothesized joint set combinations under static conditions.

Nevertheless, three possible destabilizing conditions were taken into account: (a) static water filling the joints, (b) seismic action, and (c) weathering of the joint surface.

The static action due to water filling of the joints (a) was taken into account by assuming distributions of isotropic stresses all around the block; such distributions were integrated along the joint surfaces to compute the incremental lateral forces exerted by the water. By increasing the water level within the joint, the critical conditions for the block equilibrium were determined, indicating a critical value of the water height (Zw_{cr}) that must be assumed for each wedge geometry, as summarized in Table 6. From the results of this analysis, a few tenths of a centimeter of water filling can be responsible for causing disequilibrium conditions.

Since a jointed rock mass represents a discontinuous system it is possible to identify characteristic volumes of blocks isolated by joint sets; it is also reasonable to apply to the barycenter of the rigid rock blocks that are prone to failure a destabilizing pseudo-static force in order to evaluate their stability conditions by performing a limit equilibrium analysis, i.e., to assume a co-seismic failure if the pseudo-static threshold is exceeded. The pseudo-static seismic action (b) was considered by assuming a horizontal acceleration and computing the safety factor SF according to the simplified equations of Hoek and Bray (1981):

$$\mathrm{SF} = [(R_A + R_B)\tan\varphi_{av}] / W\sin\psi_i \tag{4}$$

$$(R_A + R_B) = [(W\cos\psi_i - Wk_x\sin\psi_i)\sin\beta] / \left[(W\sin\psi_i + Wk_x\cos\psi_i)\sin(\xi/2)\right] \tag{5}$$

where W is the weight force; R_A and R_B are the resistance forces acting normally to wedge planes A and B, respectively; φ_{av} is the friction angle of the wedge joints (in this simplified equation, the value is the same for the two joints and is assumed equal to an average friction value); ψ_i is the angle of inclination of the intersection line between the two wedge planes measured with respect to the horizontal line; ξ

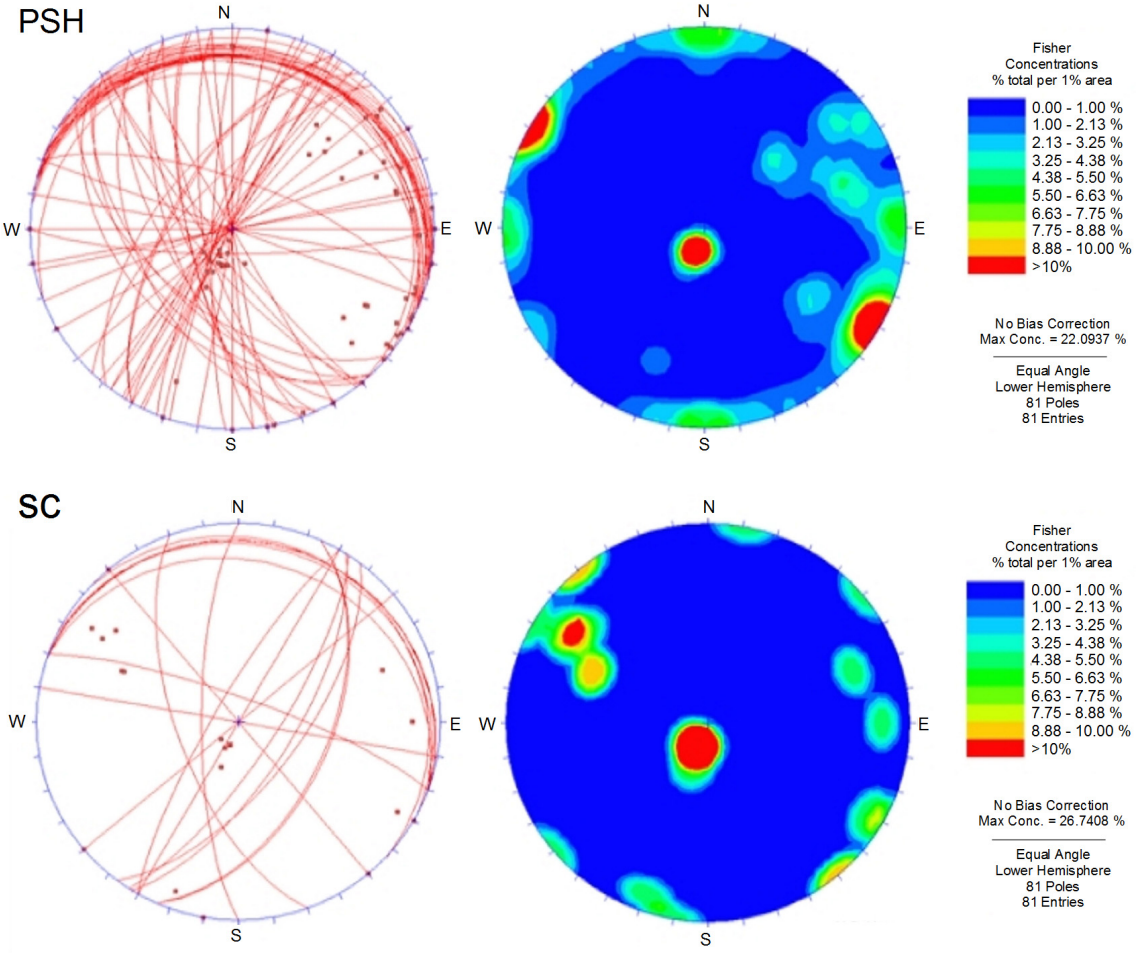

Fig. 7. Great circles and stereo plots for PSH Fm. and SC Fm. merged from the geomechanical measurements by direct and remote surveys.

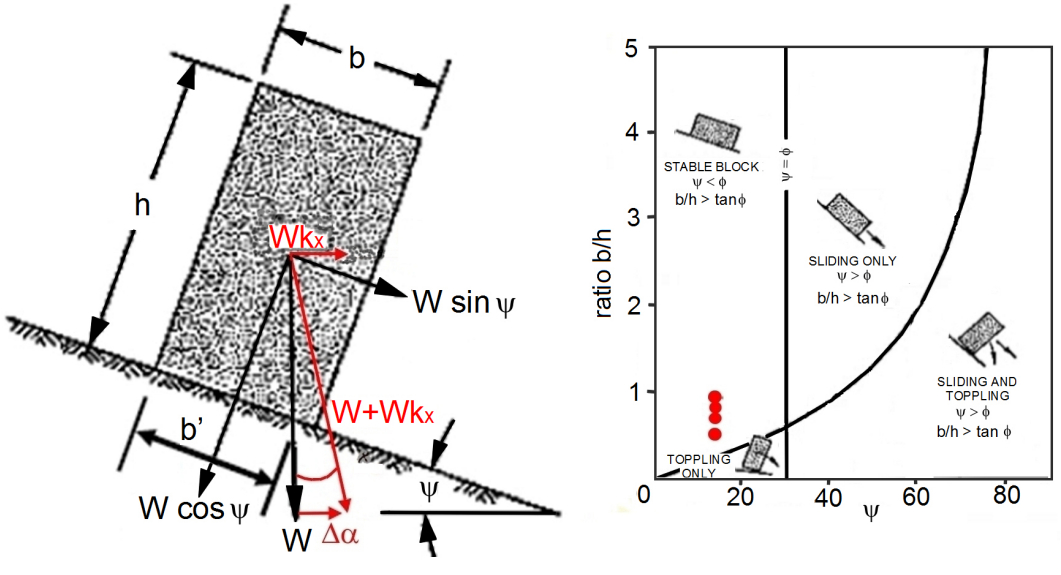

Fig. 8. Stability chart for rock topples (modified from Goodman and Bray, 1976); the red circles correspond to the rock blocks of the Mt. Pucci cliff slope.

Table 6. Stability analysis of rock wedges at Mt. Pucci: $Z\mathrm{w}_{\mathrm{cr}}$ – critical height of the static water filling the joints; k_{cr} – pseudo-static critical acceleration; SF_{475} – safety factor computed for a pseudo-static seismic action with a return time of 475 yr; $\mathrm{SF2}_{475}$ – safety factor computed for a pseudo-static seismic action with a return time of 2475 yr; $\mathrm{SF}_{r/R}$ – safety factor for weathered joint conditions (r/R is the weathering joint ratio; De Vallejo, 2005).

Slope face (dip dir/dip)	Joint sets	$Z\mathrm{w}_{\mathrm{cr}}$ (m)	k_{cr} (g)	SF_{475} yr ($k_{\mathrm{x}} = 0.169$ g)	SF_{2475} yr ($k_{\mathrm{x}} = 0.316$ g)	$\mathrm{SF}_{r/R}$ 0.2	0.4	0.6	0.8	1
300/60	J1–J4	0.38	0.07	< 1	< 1	< 1	1.2	1.5	1.7	2.6
300/60	J1–J5	0.55	0.44	1.7	1.2	1.1	1.5	1.9	2.3	3.3
320/75	J1–J2	0.2	< 0.05	< 1	< 1	< 1	< 1	1.3	1.5	2.2
320/75	J1–J4	0.48	0.46	1.8	1.3	< 1	1.2	1.5	1.8	2.6
320/75	J1–J5	0.65	0.37	1.6	1.1	1.2	1.5	1.9	2.3	3.3
345/70	J1–J2	0.4	< 0.05	< 1	< 1	< 1	1.0	1.3	1.5	2.2
345/70	J1–J4	0.48	0.48	1.9	1.4	< 1	1.2	1.5	1.8	2.6
345/70	J1–J5	0.65	0.66	2.7	1.9	1.2	1.5	1.9	2.3	3.3
355/80	J1–J2	0.5	< 0.05	< 1	< 1	< 1	1.0	1.3	1.5	2.2
355/80	J1–J4	0.58	0.50	2	1.5	< 1	1.2	1.5	1.8	2.6
355/80	J1–J5	0.65	0.78	3.1	2.1	1.1	1.5	1.9	2.3	3.3
330/70	J1–J2	0.3	< 0.05	< 1	< 1	< 1	1.0	1.2	1.5	2.2
330/70	J1–J4	0.48	0.45	1.7	1.2	< 1	1.2	1.5	1.8	2.6
330/70	J1–J5	0.55	0.36	1.5	1.1	1.2	1.5	1.9	2.3	3.3

is the wedge opening angle (measured between the dip directions of planes A and B); and k_{x} is the pseudo-static horizontal coefficient.

According to Eqs. (3) and (4), the critical pseudo-static acceleration k_{cr} was derived for each block geometry. Table 6 reports the SFs computed for the local pseudo-static horizontal acceleration corresponding to return times of 475 years and 2475 years, i.e., equal to 0.17 and 0.32 g, respectively (INGV, 2006).

With respect to (c) the weathering of the joints, a theoretical reduction in the strength values was assumed depending on the weathered friction angle φ_{wth} and computed with the following empirical equation (De Vallejo, 2005):

$$\varphi_{\mathrm{wth}} = (\varphi_{\mathrm{b}} - 20^{\circ}) + 20(r/R), \quad (6)$$

where R is the Schmidt sclerometer rebound value obtained for an intact joint, r is the Schmidt sclerometer rebound value obtained for a weathered joint, and φ_{b} is the internal friction angle of the intact rock.

The $\mathrm{SF}_{r/R}$values computed under weathered conditions (i.e., by assuming different values of the r/R weathering ratio) demonstrate that unstable conditions for the blocks are generally reached if the r/R ratio is lowered to 60 % of its max value (Table 6), i.e., corresponding to a highly significant reduction in the strength values with respect to the intact joint.

However, if a combined action due to weathering and static water filling of the joints is assumed, the computed SF values exhibit a different behavior: when a less than 60 % reduction in joint strength due to weathering is considered, unstable conditions are generally reached for water levels lower than 47 % with respect to those required to cause unstable conditions in the case of intact joints.

6 GBInSAR and IRT survey

In order to get additional information about the cliff proneness to failure we experimentally performed short-term monitoring by GBInSAR and TLS remote-sensing techniques. GBInSAR (also referred to as TInSAR) has been extensively used since the early 2000s for the monitoring of landslides (among others, Pieraccini et al., 2002; Tarchi et al., 2003; Antonello et al., 2004; Noferini et al., 2005; Bozzano et al., 2010, 2011; Intrieri et al., 2012; Crosetto et al., 2013; Bozzano et al., 2013, 2014). However, instead of the numerous studies on landslides, few applications of GBInSAR to the monitoring of landslides in coastal areas exist (Intrieri, 2013 and references therein, Hermanns et al., 2013 and references therein) and even less to the analysis of rock cliffs (Mazzanti and Brunetti, 2010). Furthermore, few studies have been done on the rigorous integration of GBInSAR maps with TLS point clouds in order to achieve an easier and correct visualization of GBInSAR maps (Tapete et al., 2013).

On the other hand, IRT has been used, especially in the last few years, for characterizing rock masses and their jointing conditions (Gigli et al., 2013; Teza et al., 2013).

A comprehensive description of the GBInSAR and IRT surveys performed, data analysis and results is presented below.

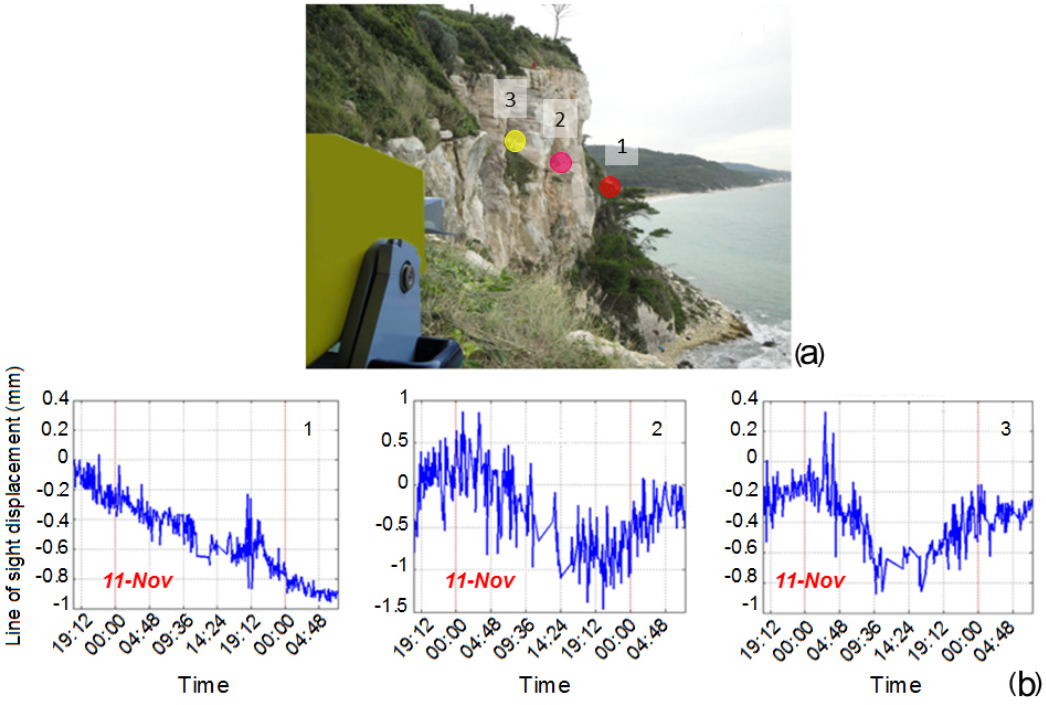

Fig. 9. (a) picture showing the GBInSAR interferometer installed in the east of the Mt. Pucci cliff slope; **(b)** time series of displacements of three points located on the cliff (colored circles identify the corresponding point locations on the cliff slope). Coordinates of the three points (Lat and Long in WGS84 and Elevation in m a.s.l.): (1) Lat 15°59′22.75″, Long 41°56′44.28″, Elevation 25.3; (2) Lat 15°59′25.59″, Long 41°564′45.33″, Elevation 46.9; (3) Lat 15°59′26.25″, Long 41°56′45.50″, Elevation 48.7.

6.1 GBInSAR survey

A continuous GBInSAR monitoring survey with a sampling rate of about five minutes was performed from 10 November to 12 November 2010, using Ku band IBIS-L SAR equipment, manufactured by IDS S.p.A., installed in front of the Mt. Pucci cliff at distances ranging from 80 to 150 m (Fig. 4). 442 SAR (synthetic aperture radar) maps characterized by a range and cross-range resolution of approximately 0.5×0.5 m were collected over the entire monitoring period.

The overall SAR data set was analyzed by using standard differential and multi-image processing methods (Luzi, 2010) and by the advanced "PtoP approach" specifically developed by Mazzanti and Brunetti (2010) for the analysis of rock masses. By this approach, atmospheric phase contribution is removed by alternatively positioning ground control points (GCP) on the different rock mass sectors across the main joints and, thus, computing local differential displacements, by assuming a negligible atmospheric phase variation. By this processing approach, the eventual displacement of the overall cliff is neglected and the analysis is only focused on localized anomalies that can be detected with a decimal mm accuracy.

Considering the unfavorable positioning of the SAR system with respect to the cliff orientation (anyway the only one where installation was feasible), and the potential coarse ground range resolution due to foreshortening effects, a dedicated georeferencing survey by an artificial corner reflector alternatively positioned on the cliff during the SAR acquisition time was performed. Data collected during the georeferencing survey allowed us to overlay the 2-D interferogram rigorously onto the 3-D point cloud with a precision of less than 1 m.

Micro-movements affecting the cliff were detected during the 3 days of monitoring, presumably ascribable to thermal effects on released blocks, even if no direct control data are available to support this hypothesis. However, such data were useful for identifying and localizing portions of the cliff affected by micro-movements (Fig. 9).

6.2 IRT survey

IRT surveys were performed from 10 November to 12 November 2010, using a NEC TH7700 camera characterized by a low 320×240 pixel resolution (corresponding to about 0.5 to 1 m resolution on the cliff) and a nominal accuracy of 0.1 °C. Thermal images were collected at different times from two different sensing sites (Fig. 4), thus achieving wider coverage of the overall cliff and allowing us to investigate the thermal variations of the cliff under different sunlight conditions. Both absolute temperature (Fig.10) and thermal changes with time were obtained. Images were firstly cor-

Fig. 10. Thermal static map obtained by IRT remote surveys of the overall Mt. Pucci cliff slope.

rected for geometric distortions by traditional methods based on ground reference points and then overlaid with optical images collected by high-resolution photo camera by achieving an overlapping accuracy ranging from a few cm to a few tenths of cm depending on the different location portions of the cliff (due to the different geometry of the cliff, the different perspective conditions and the distance from the viewpoints). Anyway, it is worth noting that the mean overlapping value is below the pixel resolution accuracy of the thermal images. By a simple dedicated MATLAB algorithm differential values were computed for each pixel among images collected at different times.

Mean temperatures ranging from 10 to 18 °C were found in different sectors of the cliff (Fig. 10), while differential values on the same sectors did not exceed the value of 3 °C.

7 Discussion

At the Mt. Pucci sea cliff direct traditional geomechanical survey and remote measurements were integrated to perform a geostructural survey that led to a slope stability analysis focused on rock topples and wedge block sliding.

A comparison between Tables 1 and 3 shows that the joint set data derived from traditional field surveys and from traditional geomechanical scanlines are quite similar, except for the secondary joint set J2 for the SC Fm. This difference may be related to the distance between the unique available field geomechanical station on the SC Fm. and the Mt. Pucci sea cliffs (Fig. 2). As a matter of fact, the inaccessibility of the cliff and the geological setting of the area did not allow to find SC Fm. outcrops close enough to the investigated area in order to be assumed as not affected by local structural controls (see Fig. 2). These results confirm the reliability of geostructural results derived from the TLS data analysis and the importance of integrating field measurements and TLS data both for complementing the information and for cross-checking the validity of achieved results.

Moreover, short-term monitoring via GBInSAR and IRT pointed out the role of the surveyed joint sets in inducing instabilities in the sea cliff, as the thermal images allowed for the identification of certain positive and negative anomalies that correspond to the main joints and to parts of the cliff slope affected by recent collapses, i.e., corresponding to clearly visible scars. A similar application of the IRT was experienced also to historical buildings for detecting discontinuities beneath the surface, such as windows, fractures, structural connections or thinner cover (Fanou et al., 2012); the structural discontinuities were associated with the observed thermal anomalies, i.e., not considering the absolute value of the measured temperatures on the building faces, and they were interpreted as a sort of difference in heat efficiency by the building structure.

According to Jaboyedoff et al. (2012), these results confirm the reliability of remote geostructural surveys to constrain rock slide geometries well; in this way they contribute to forecasting possible rock failure mechanisms and to evaluating the stability conditions of the rock masses prone to failure (Zhang et al., 2010). Nevertheless, remote surveys are commonly applied to mountain cliff slopes (Jaboyedoff et al., 2007; Oppikofer et al., 2009; Sturzenegger and Stead, 2009), where a more appropriate view of the cliff can be achieved. On the opposite, sea cliffs are generally scanned from a lateral point of view and such an unfortunate view can reduce the efficacy of both geometric reconstruction of the cliff and joint set identification and characterization. The combination of manual and supervised automatic detection of joint surfaces by the operator on the TLS-derived point cloud has been demonstrated to be effective for the identification of surfaces not clearly detectable by the fully automatic analysis. Moreover, to perform the slope stability analyses mechanical properties are requested that cannot be provided by remote survey. For the above reasons, this work confirms that an integrated approach combining direct and remote surveys is necessary to provide a good and reliable geostructural rock mass characterization.

Looking at the Mt. Pucci cliff, as it resulted from the geostructural surveys, rock topples and rock wedge sliding can be expected, as also demonstrated by the observed shape of the detachment areas corresponding to recently fallen blocks.

Based on the geostructural constraints, typical geometries for topples and wedge blocks were derived and pseudo-static as well as hydrostatic destabilizing forces were considered (i.e., representative of effects related to seismic waves and water filling the joints). Moreover, since the Mt. Pucci slope is also exposed to sea water atomized by the waves breaking at the bottom of the cliff, a strength reduction due to the weathering was considered.

The results from the performed stability analyses showed that several blocks could potentially lead to instability

conditions. The coupled GBInSAR and IRT monitoring was herein used as an additional source of information useful to better prioritize potentially unstable blocks and sectors of the cliff on the basis of additional indicators of stability (i.e., micro-movements, thermal anomalies). The high accuracy of micro-movements detectable by the GBInSAR system by using the "PtoP" processing approach can be very useful for identifying indicators of displacement related to external agents (e.g., temperature). However, on the other hand, we cannot neglect that the unfavorable sensing position of the GBInSAR system significantly reduces its efficacy in detecting displacement as the LOS (line of sight) is significantly inclined with respect to the expected movement of the rock mass. This point has several implications for the application of GBInSAR measurements for the investigation of sea coastal cliffs. In spite of the above-mentioned limitation, cyclic LOS movements with a daily base ranging from 0.5 to 1.2 mm were detected at certain locations and tentatively attributed to the thermal variation of the rock mass due to different sunlight conditions. Cyclic movements could lead to local failures (Vlcko et al., 2009; Hatzor and Bakun Mazor, 2013) when combined with destabilizing actions (i.e., earthquakes, water pressures) or conditions (i.e., strength reduction for weathering), as suggested by the performed slope stability analyses.

Thermal images collected by IRT can be qualitatively used to support the above-mentioned hypothesis. As a matter of fact, the comparison between Figs. 5 and 10 shows that a high concentration of thermal anomalies (i.e., positive and negative values with respect to the mean value) corresponds to the western portion of the sea cliff affected by recent detachments of blocks. Moreover, another relevant thermal anomaly coincides with a wide detachment area, i.e., where the block failure already occurred.

The findings reported here lead to the suggestion that the experienced monitoring techniques can contribute to both the available approaches devoted to risk management: (i) the "deterministic approach" that consists on analyzing the recorded data with respect to a geological model of the natural system (Angeli et al., 2000; Prestininzi et al., 2012) and providing different levels of sensitivity with respect to possible failure or yielding scenarios; (ii) the "statistical approach" that consists on carrying out a cloud multiparametric analysis (a multisource strategy of investigation) by analyzing all of the collected data in terms of anomaly recurrence (Travelletti et al., 2008; Bigarrè et al., 2011) and associating the critical conditions of the natural system with these anomalies, i.e., without relating them to an interpretative model but strongly constraining it by the redundancy of the independent records.

Regarding the deterministic approach, as the cliff gradually evolves toward a coastal slope, the landslide mechanisms change, and the existence of an emerged beach favors monitoring with remote techniques. More in particular, the GBInSAR and IRT remote monitoring applied here can be helpful for better constraining the failure mechanism if they are integrated among them so providing suitable indications on the location of possible failure occurrence (Blikra et al., 2005; Bornhold and Thomson, 2012).

Moreover, remote sensing devices installed on sea cliffs could be efficiently associated to direct precursor monitoring systems (Amitrano et al., 2005; Senfaute et al., 2009; Wust-Block, 2010; Lenti et al., 2012) to detect the temporal evolution of instability processes in order to frame the integrated operating systems within alert strategy for real-time prevention.

8 Conclusions

The present study demonstrates the reliability of an integrated approach to the geomechanical characterization of rock sea cliffs for the analysis of slope stability conditions. To this end, a detailed analysis of the 45 m-high Mt. Pucci sea cliff (Gargano promontory, Italy) was performed using different survey techniques and analytical stability methods.

The combination of traditional geomechanical surveys and remote geostructural investigations using a TLS point cloud allowed us to produce a comprehensive and affordable characterization of the main joint sets, which leads to the identification of the kinematic proneness to rock failures and to the constraint of the reliable failure mechanisms for performing slope stability analyses.

Independent evidence of ongoing effects (i.e., displacements) or conditioning factors (i.e., joint concentration or anomalies in the rock mass property distribution) were investigated by integrating GBInSAR and IRT techniques.

The performed slope stability analysis showed that the Mt. Pucci sea cliff is prone to rock failures mainly consisting in topples and wedge sliding, while no kinematic compatibility exists with sliding rock failures. SFs were computed by taking into account the weathering of the joints and the hydrostatic pressure due to water filling the opened cracks as well as in the case of local pseudo-static horizontal acceleration corresponding to return times of 475 and 2475 years. Moreover, as it results from the stability analysis performed by assuming a combined action due to weathering and static water filling the joints, if a less than 60 % reduction of joint strength due to weathering is considered, unstable conditions are generally reached for water levels lower than 47 % with respect to those required to cause unstable conditions in the case of intact joints.

The Mt. Pucci case study pointed out the complexity and limitations of the use of terrestrial remote sensing in coastal environments due to the partial and side visibility of the cliffs. Nevertheless, the obtained results lead to a promising perspective in the integrated application of remote monitoring techniques for the investigation of coastal cliffs. They also encourage the integration of remote-sensing devices with other typologies of monitoring systems (such as the

micro-seismic and geotechnical ones) for an early-warning strategy applied to sea cliff slopes.

Acknowledgements. The authors wish to thank A. Brunetti and Geoservizi S.r.l. for their technical support to the monitoring; A. Bretshneider and M. Savina for their contribution on collecting and processing the survey data; A. Argento for the figure design; P. Tarolli for his useful revisions.

Edited by: P. Tarolli
Reviewed by: four anonymous referees

References

Amitrano, D., Grasso, J. R., and Senfaute, G.: Seismic precursory patterns before a cliff collapse and critical point phenomena, Geophys. Res. Lett., 32, L08314, doi:10.1029/2004GL022270, 2005.

Angeli, M.G., Pasuto, A., and Silvano, S.: A critical review of landslide monitoring experiences, Engin. Geol., 55, 133–147, 2000.

Antonello, G., Casagli, N., Farina, P., Leva, D., Nico, G., Siebar, A. J., and Tarchi, D.: Ground-based SAR interferometry for monitoring mass movements, Landslides, 1, 21–28, 2004.

ASTM D5731-08: Standard Test Method for Determination of the Point Load Strength Index of Rock and Application to Rock Strength Classifications.

Assier-Rzadkiewicz, S., Heinrich, P., Sabatier, P. C., Savoye, B., and Bourillet, J. F.: Numerical modelling of landslide-generated tsunami: the 1979 Nice event, Pure Appl. Geophys., 157, 1707–1727, 2000.

Barton, N.: Rewiew of a new shear strength criterion for rock joints. Engineering Geology, Elsevier, 7, 287 – 332, 1973.

Barton, N. and Bandis, V.: Review of predictive capabilities of JRC – JCS model in engineering practice. Proceeding of Int. Symposium of rock joint, Loen, Norway, Balkema, 603–610, 1990.

Baul, R. L. and Godt, J. W.: Early warning of rainfall-induced shallow landslides and debris flows in the USA, Landslide, 7, 259–272, 2010.

Bigarré, P., Klein, E., Gueniffey, Y., and Verdel, T.: Cloud monitoring: an innovative approach for the prevention of landslide hazards. The Second World Landslide Forum Rome, 2011. Abstracts Book WLF2, L16, 475 (free download from the website: www.wlf2.org/home/proceedings/WLF2_Abstract_Book_2011.pdf), 2011.

Billi, A. and Salvini, F.: Sistemi di fratture associati a faglie in rocce carbonatiche: nuovi dati sull'evoluzione tettonica del Promontorio del Gargano, Boll. Soc. Geol. It., 119, 237–250, 2000.

Blikra, L. H.: The Aknes rockslide, Norway, in Landslides – Types, Mechanisms and Modeling, edited by J. J. Clague and D. Stead, 323–335, Cambridge University Press, Cambridge, UK, 2012.

Blikra, L. H., Longva, O., Harbitz, C., and Løvholt, F.: Quantification of rock avalanche and tsunami hazard in Storfjorden, western Norway, in: Landslide and Avalanches, edited by: Sennest, K., Flaate, K., and Larsen, J. O., Taylor and Francis Group, London, UK, 7–63, 2005.

Bornhold, B. D. and Thomson, R. E.: Tsunami hazard assessment related to slope failures in coastal waters, in: Landslides – Types, Mechanisms and Modeling, edited by: Clague, J. J. and Stead, D., Cambridge University Press, 108–120, 2012.

Bosellini, A. and Morsilli, M.: A lower Cretaceus drawing unconformity on the eastern flank of the Apulia Platform (Gargano Promontory, Southern Italy), Cretaceaus Research, Belfast, 18, 51–61, 1997.

Bosellini, A. and Morsilli, M.: Il Promontorio del Gargano: cenni di geologia ed itinerari geologici, Quaderni del Parco Nazionale del Gargano, 1–48, 2001.

Bosellini, A., Morsilli, M., and Neri, C.: Long-term event stratigraphy of the Apulia Platform Margin (Upper Jurassic to Eocene, Gargano, Southern Italy), Journal of Sedimentary Research, Tulse, 69/6, 1241–1252, 1999.

Bozzano, F., Mazzanti, P., Prestininzi, A., and Scarascia Mugnozza, G: Research and development of advanced technologies for landslide hazard analysis in Italy, Landslides, 7, 381–385, 2010.

Bozzano, F., Cipriani, I., Mazzanti, P., and Prestininzi, A.: Displacement patterns of a landslide affected by human activities: insights from ground-based InSAR monitoring, Natural Hazards, 59, 1377–1396, doi:10.007/s11069-011-9840-6, 2011.

Bozzano, F., Lenti, L., Martino, S., Montagna, A., and Paciello, A.: Earthquake-triggering of landslides in highly jointed rock masses: the 1783 Scilla rock avalanche (Italy), Geomorphology, 129, 294–308. 2011a.

Bozzano, F., Cipriani, I., Mazzanti, P., Prestininzi, A.: A field experiment to calibrate landslide time of failure prediction functions, International Journal of Rock Mechanics and Mining Sciences, 67, 69–77, 2014.

Bozzano, F, Cipriani, I., Martino, S., Mazzanti, P., and Prestininzi, A.: Forecasting methods for landslides interacting with infrastructures, Landslide Science and Practice, edietd by: Margottini, C., Canuti, P., and Sassa, K., Social and Economic Impact and Policies, 6, 247–254, 2013.

Bregoli, F., Bateman Pinzon, A., Medina Iglesias, V., and Gomez Cortes, D.: Experimental studies on 3-D impulsive waves generated by rapid landslides and debris flows, in: International Conference on Vajont 1963–2013: Thoughts and analyses after 50 years since the catastrophic landslide, edited by: Genevois, R. and Prestininzi, A., 115–122, 2013.

Cipriani, I. and Mazzanti, P.: Analisi del comportamento deformativi pre-rottura di frane superficiali tramite monitoraggio con Interferometria SAR Terrestre, Eng. Hydro. Env. Geology., 14B, 66–67, 2012.

Crosetto, M., Gili, J. A., Monserrat, O., Cuevas-González, M., Corominas, J., and Serral, D.: Interferometric SAR monitoring of the Vallcebre landslide (Spain) using corner reflectors, Nat. Hazards Earth Syst. Sci., 13, 923–933, doi:10.5194/nhess-13-923-2013, 2013.

Della Seta, M., Martino, S., and Scarascia Mugnozza, G.: Quaternary sea-level change and slope instability in coastal areas: Insights from the Vasto Landslide (Adriatic coast, central Italy), Geomorphology, 201, 468–478, 2013.

De Vallejo, L. G.: Geoingegneria, Pearson Education Italia S.r.l., Milano, 2005.

De Vita, P., Cevasco, A., and Cavallo, C.: Detailed rock failure susceptibility mapping in steep rocky coasts by means of non-contact geostructural surveys: the case study of the Tigullio Gulf (Eastern Liguria, Northern Italy), Nat. Hazards Earth Syst. Sci., 12, 867–880, doi:10.5194/nhess-12-867-2012, 2012.

Dewez, T. J. B., Rohmer, J., Regard, V., and Cnudde, C.: Probabilistic coastal cliff collapse hazard from repeated terrestrial laser surveys: Case study from Mesnil Val (Normandy, northern France), J. Coast. Res., Spec. Issue, 65, 702–707, 2013.

Dickson, M. E., Ogawa, H., Kench, P. S., and Hutchinson, A.: Seacliff retreat and shore platform widening: Steady-state equilibrium?, Earth Surf. Proc. Landforms, 38, 1046–1048, 2013.

DISS Working Group: Database of Individual Seismogenic Sources (DISS), Version 3.1.1: A compilation of potential sources for earthquakes larger than M 5.5 in Italy and surrounding areas, http://diss.rm.ingv.it/diss/, ©INGV 2010 – Istituto Nazionale di Geofisica e Vulcanologia – All rights reserved, 2010.

Duncan, C. W. and Christopher, W. M.: Rock Slope Engineering: Civil and Mining, Taylor & Francis, 431 pp., 2004.

Duperret, A., Genter, A., Martinez, A., and Mortimore, R. N.: Coastal chalk cliff instability in NW France: the role of lithology, fracture pattern and rainfall, in: Coastal chalk Cliff Instability, edited by: Mortimore, R. N. and Duperret A., Geological Society, London, Eng. Geol. Sp., 20, 33–55, 2004.

Duperret, A., Genter, A., Martinez, A., Mortimore, R. N., Delacourt, B., and Pomerai, M. R.: Coastal Rock Cliff Erosion by Collapse at Puys, France: The Role of Impervious Seams within Chalk of NW Europe, J. Coastal Res., 18, 52–61, 2002.

Emery, K. O. and Kuhn, G. G.: Sea cliffs: their processes, profiles, and classification. Geological Society America Bulletin, 93, 644–654, 1982.

Epifanio, B., Zezere, J. L., and Neves, M.: Identification of hazardous zones combining cliff retreat rates with landslide susceptibility assessment, J. Coast. Res., 65, 1681–1686, 2013.

Fanou, S. S., Kauppinen, T., Bartoccini, P., Colucci, A., Di Biagio, F., Di Sarcina, C., Fasano, G., Labia, N., Martini, E., Maso, R., Poggi, M., and Tati, A.: Energy-related innovative concepts, methods and techniques for suistainable protection and conservation of historic buildings in urban areas. In: Clemente P., Di Lazzaro P. and Giorgi R. eds., Knowledge, diagnostic and preservation of cultural heritage, EAI (ENEA) Special Volume (II-2012), 101–110, 2012.

Federico, A., Popescu, M., Elia, G., Fidelibus, C., Interno, G., and Murianni, A.: Prediction of time to slope failure: a general framework, Environ. Earth Sci., 66, 245–256 2012.

Fine, I. V., Rabinovich, A. B., Bornhold, B. D., Thomson, R. E., and Kulikov, E. A.: The Grand Banks landslide-generated tsunami of November 18, 1929; preliminary analysis and numerical modeling, Mar. Geol. 215, 45–57, 2005.

Force, E. R.: Sea cliff erosion within rising sea-level along shores exposing glacial material in Atlantic Canada: the effect of bedrock slope and an example from Isle Madame, Nova Scotia, Proc. Roy. Soc. B., 280, 32–39, 2013.

Fortunato, C., Martino, S., Prestininzi, A., and Romeo, R. W.: New release of the Italian catalogue of earthquake-induced ground failures (CEDIT), Ital. J. Engin. Geol. Environ., 2, 63–74, 2012.

Fuhrmann, C. M., Konrad, C. E., and Band, L. E. : Climatological Perspectives on the Rainfall Characteristics Associated with Landslides in Western North Carolina, Phys. Geogr., 29, 289–305, 2008.

Gaffet, S., Guglielmi, Y., Cappa, F., Pambrun, C., Monfret, T., and Amitrano, D.: Use of the simultaneous seismic, GPS and meteorological monitoring for the characterization of a large unstable mountain slope in the southern French Alps, Geophys. J. Int., 182, 1395–1410, 2010.

Gigli, G., Frodella, W., Garfagnoli, F., Morelli, S., Mugnai, F., Menna, F., and Casagli, N.: 3-D geomechanical rock mass characterization for the evaluation of rockslide susceptibility scenarios, Landslides, 1–10, 2013.

Goodman, R. E. and Bray, J. W.: Toppling of rock slopes In: Rock engineering for foundations and slopes; proceedings of a specialty conference, Am. Soc. Civ. Eng., New York, 2, 201–233, 1976.

Hampton, M. A., Griggs, G. B., Edil, T. B., Guy, D. E., Kelley, J. T., Komar, P. D., Mickelson, D. M., and Shipman, H. M.: Processes that Govern the Formation and Evolution of Coastal Cliffs, in: Formation, Evolution, and Stability of Coastal Cliffs–Status and Trends, edited by: Hampton, M. A. and Griggs, G. B., USGS – Professional Paper 1693, 1–4, 2004.

Hatheway, H. W.: The Complete ISRM Suggested Methods for Rock Characterization, Testing and Monitoring, 1974–2006, Environ. Engin. Geosci., 15, 47–48, 2009.

Hatzor, Y. and Bakun-Mazor, D.: Thermally vs. seismically induced block displacements in jointed rock slopes, in: International Conference on Vajont 1963–2013: Thoughts and analyses after 50 years since the catastrophic landslide, edited by: Genevois, R. and Prestininzi, A., 41–49, 2013.

Heezen, B. C. and Ewing, M.: Turbidity currents and submarine slumps, and the 1929 Grand Banks Earthquake, Am. J. Sci., 250, 849–873, 1952.

Hermanns, R. L., Blikra, L. H., Anda, E., Saintot, A., Dahle, H., Oppikofer, T., Fischer, L.: Systematic mapping of large unstable rock slopes in Norway, in: Landslide Science and Practice, Springer Berlin Heidelberg, 29–34, 2013.

INGV: Mappa di pericolosità sismica del territorio nazionale, available at: http://esse1.mi.ingv.it/, 2006.

Intrieri, E., Gigli, G., Mugnai, F., Fanti, R., and Casagli, N.: Design and implementation of a landslide early warning system, Engin. Geol., 147–148, 124–136 doi:10.1016/j.enggeo.2012.07.017, 2012.

Intrieri, E., Di Traglia, F., Del Ventisette, C., Gigli, G., Mugnai, F., Luzi, G., and Casagli, N.: Flank instability of Stromboli volcano (Aeolian Islands, Southern Italy): integration of GBInSAR and geomorphological observations, Geomorphology, 201, 60–69, 2013.

ISPRA: Atlante Italiano delle Coste, http://www.isprambiente.gov.it/it/servizi-per-lambiente/stato-delle-coste/atlante-delle-coste, 2012.

ISRM: Suggested Methods for Determining Water Content, Porosity, Density, Absorption and Related Properties and Swelling and Slake-Durability Index Properties, 1977.

ISRM: Suggested methods for the quantitative description of discontinuities in rock masses, International Journal of Rock Mechanics Mining Sciences & Geomechanics, 1978.

ISRM: Suggested Methods for Determining Point Load Strength, International Society for Rock Mechanics Commission on Testing Methods, Int. J. Rock. Mech.Min. Sci. and Geomechanical Abstr., 22, 51–60, 1985.

ISRM: The Complete ISRM Suggested Methods for Rock Characterization, Testing and Monitoring: 1974–2006, Suggested Methods Prepared by the Commission on Testing Methods, International Society for Rock Mechanics, edited by: Ulusay, R. and

Hudson, J. A., Compilation Arranged by the ISRM Turkish National Group, Ankara, Turkey, 628 pp., 2007.

Jaboyedoff, M., Metzger, R., Oppikofer, T., Couture, R., Derron, M. H., Locat, J. and Turmel, D.: New insight techniques to analyze rock-slope relief using DEM and 3D-imaging cloud points: COLTOP-3D software, in: Rock mechanics: Meeting Society's Challenges and demands (Vol. 1), edited by: Eberhardt, E., Stead, D., and Morrison, T., Taylor & Francis, 61–68, 2007.

Jaboyedoff, M., Derron, M. H., Jakubowski, J., Oppikofer, T., and Pedrazzini, A.: The 2006 Eiger rockslide European Alps, in: Landslides – Types, Mechanisms and Modeling, edited by: Clague, J. J. and Stead, D., Cambridge University Press, Cambridge, UK, 282–296, 2012.

Katz, O. and Mushkin, A.: Characteristic of sea cliff erosion induced by a strong winter storm in eastern Mediterranean, Quat. Res. USA, 80, 20–32, 2013.

Lai, X. P., Cai, M. F., and Xie, M. W.: In situ monitoring and analysis of rock mass behavior prior to collapse of the main transport roadway in Linglong Gold Mine, China, Int. J. Rock Mechan. Mining Sci., 43, 640–646, 2006.

Lee, E. M., Hall, J. W., and Meadowcroft, I. C.: Coastal cliff recession: the use of probabilistic prediction methods, Geomorphology, 40, 253–269, 2001.

Lee, E. M., Meadowcroft, I. C., Hall, J. W., and Walkden, M.: Coastal landslide activity: a probabilistic simulation model, B. Eng. Geol. Environ., 61, 347–355, 2002.

Lenti, L., Martino, S., Paciello, A., Prestininzi, A., and Rivellino, S.: Microseismicity within a karstified rock mass due to cracks and collapses triggered by earthquakes and gravitational deformations, Natural Hazards, 64, 359–379, 2012.

L'Heureux, J. S., Eilertsen, R. S., Glimsdal, S., Issler, D., Solberg, I. L., and Harbitz, C. B.: The 1978 quick clay landslide at Rissa, mid Norway: subaqueous morphology and tsunami simulations. In Proceedings of the 5th International Symposium on Submarine Mass Movements and Their Consequences, edited by: Yamada, Y., Kawamura, K., and Ikehara, K, Kyoto, Japan, Springer Science + Business Media, 2011.

Lim, D. I., Choy, J. Y., and Hung, H. S.: Sea cliff erosion and retreat in semi-enclosed macrotidal embayment: Hampyung bay, west coast of Corea. Journal of Coastal Research, Spec. Issue, 56, 732–736, 2009.

Lim, M., Rosser, N. J., Allison, R. J., and Petley, D. N.: Erosional processes in the hard rock coastal cliffs at Staithes, North Yorkshire, Geomorphology, 114, 12–21, 2010.

Loew, S., Gischig, V., Willenberg, H., Alpiger, A., and Moore, J.: Randa: Kinematics and driving mechanisms of a large complex rockslide, in Landslides – Types, Mechanisms and Modeling, edited by: J. J. Clague and D. Stead, Cambridge University Press, Cambridge, UK, 297–309, 2012.

Mantovani, M., Devoto, S., Forte, E., Mocnik, A., Pasuto, A., Piacentini, D., and Soldati, M.: A multidisciplinary approach for rock spreading and block sliding investigation in the northwesterncoast of Malta, Landslides, 10, 611–622, 2013.

Markland, J. T.: A useful technique for estimating the stability of rock slopes when the rigid wedge slide type of failure is expected: Imperial College Rock Mechanics Research Reprints, p. 19, 1972.

Marques, F., Matildes, R., and Redweik, P.: Statistically based sea cliff instability hazard assessment of Burgau-Lagos coastal section (Algarve, Portugal), J. Coast. Res., Special Issue 64, 927–931, 2011.

Marques, F. M. S. F., Matildes, R., and Redweik, P.: Sea cliff instability susceptibility at regional scale: a statistically based assessment in the southern Algarve, Portugal, Nat. Hazards Earth Syst. Sci., 13, 3185–3203, doi:10.5194/nhess-13-3185-2013, 2013.

Marques, F. M. S. F.: Magnitude-frequency of sea cliff instabilities, Nat. Hazards Earth Syst. Sci., 8, 1161–1171, doi:10.5194/nhess-8-1161-2008, 2008.

Mazzanti, P. and Bozzano, F.: Revisiting the February 6th 1783 Scilla (Calabria, Italy) landslide and tsunami by numerical simulation, Mar. Geophys. Res., 32, 273–286. 2011.

Mazzanti, P. and Brunetti, A.: Assessing rockfall susceptibility by Terrestrial SAR Interferometry, in: Proceedings of the Mountain Risks International Conference, edited by: Malet, J. P., Glade, T., and Casagli, N. Firenze, Italy, 24–26 November 2010, 109–114, 2010.

McCullough, M. C., Kareem, A., Donahue, A. S., and Westerink, J. J.: Structural damage under multiple hazards in coastal environments, J. Distas. Res., 8, 1042–1051, 2013.

Miller, A., Richards, J. A., McCann, D. M., Browitt, C. W. A., and Jackson, P. D.: Microseismic techniques for monitoring incipient hazardous collapse conditions above abandoned limestone mines, Quart. J. Engin. Geol., London, 22, 1–18, 1989.

Montoya-Montes, I., Rodríguez-Santalla, I., Sánchez-García, M. J., Alcántara-Carrió, J., Martín-Velázquez, S., Gómez-Ortiz, D., and Martín-Crespo, T.: Mapping of landslide susceptibility of coastal cliffs: The Mont-Roig del Camp case study, Geol. Acta, 10, 439–455, 2012.

Mortimore, R. N., Lawrence, J., Pope, D., Duperret, A., and Genter, A.: Coastal cliff geohazards in weak rock: The UK chalk cliffs of Sussex, edited by: Mortimore, R. N. and Duperret, A., in: Coastal chalk cliff instability, Geological Society, London, Eng. Geol. Sp., 20, 3–31, 2004.

Noferini, L., Pieraccini, M., Mecatti, D., Macaluso, G., and Atzeni, C.: Long term landslide monitoring by Ground Based SAR Interferometer, International J. Remote Sens., 27, 1893–1905, 2005.

Oppikofer, T., Jaboyedoff, M., Blikra, L., Derron, M.-H., and Metzger, R.: Characterization and monitoring of the Åknes rockslide using terrestrial laser scanning, Nat. Hazards Earth Syst. Sci., 9, 1003–1019, doi:10.5194/nhess-9-1003-2009, 2009.

Papadopoulos, G. A. and Kortekaas, S.: Characteristics of landslide generated tsunamis from observational data, in: Submarine Mass Movements and their Consequence, Advances in Natural and Technological Hazards Research, edited by: Locat, J. and Mienert, J., Kluwer Academic Publishers, 19, 267–374, 2003.

Paskaleva, I., Aronov, A. G., Seroglazov, R. R., and Aronova, T. I.: Characteristic features of induced seismic processes in mining regions exemplified by the potassium salt deposits in Belarus and Bulgaria, Acta Geod. Geoph. Hung, 41, 293–303, 2006.

Pennetta, M. and Russo, E. L.: Hazard factors in high rocky coasts of Capri Island (Gulf of Naples, Italy), J. Coast. Res., 61, 428–434, 2011.

Phillips, W. S., Pearson, D. C., Edwards, C. L., and Stump, B. W.: Microseismicity Induced by a Controlled, Mine Collapse at White Pine, Michigan. International Journal of Rock Mechanics & Mining Sciences, 34, 246 pp., 1997.

Pieraccini, M., Casagli, N., Luzi, G., Tarchi, D., Mecatti, D., Noferini, L., and Atzeni, C.: Landslide monitoring by ground-

based radar interferometry: a field test in Valdarno (Italy), Internat. J. Remote Sens., 24, 1385–1391, 2002.

Polemio, M., Di Cagno, M., and Virga, R.: Le acque sotterranee del Gargano: risorse idriche integrative e di emergenza, Acque sotterranee, 68, 41–58, 2000.

Prestininzi, A., Bianchi-Fasani, G., Bozzano, F., Esposito, C., Martino, S., Mazzanti, P., and Scarascia-Mugnozza, G.: From the refinement of geological models to risk management: The role of landslide monitoring, Landslides and Engineered Slopes: Protecting Society through Improved Understanding, edited by: Eberhardt, E., Froese, C., Turner, K. and Leroueil, S., Taylor & Francis Group, London, 2012.

Santos Jr., O. F., Scudelari, A. C., Costa, Y. D., and Costa, C. M.: Sea cliff retreat mechanisms in Northeastern Brazil. Journal of Coastal Research, 64, 820–824, 2011.

Senfaute, G., Chambon, C., Bigarre, P., Guise, Y., and Josien, J. P.: Spatial distribution of mining tremors and the relationship to rockburst hazard, Pure Appl. Geophys., 150, 3–4, 1997.

Senfaute, G., Abdul Wahed, M., Lenhard, F., and Morel, J.: Technique d'écoute microsismique appliquée au risqué d'effondrement dans les mines du bassin ferrifère lorrain, Revue Française de Géotechnique, 92, 57–62, 2000.

Senfaute, G., Duperret A., and Lawrence, J. A.: Micro-seismic precursory cracks prior to rock-fall on coastal chalk cliffs: a case study at Mesnil-Val, Normandie, NW France. Nat. Hazards Earth Syst. Sci., 9, 1625–1641, 2009, http://www.nat-hazards-earth-syst-sci.net/9/1625/2009/.

Schulz, W. H., Galloway, S. L., and Higgins, J. D.: Evidence for earthquake triggering of large landslides in coastal Oregon, USA, Geomorphology, 141/142, 88–98, 2012.

Stanchev, H., Young, R., and Stanckeva, M.: Integrating GIS and high resolution orthophoto images for the development of a geomorphic shoreline classification and risk assessment-a case study of cliff/bluff erosion along the Bulgarian coast, J. Coast. Conserv., 1–10, 2013.

Sturzenegger, M. and Stead, D.: Quantifying discontinuity orientation and persistence on high mountain rock slopes and large landslides using terrestrial remote sensing techniques, Nat. Hazards Earth Syst. Sci., 9, 267–287, 2009, http://www.nat-hazards-earth-syst-sci.net/9/267/2009/.

Tapete, D., Casagli, N., Luzi, G., Fanti, R., Gigli, G., and Leva, D.: Integrating radar and laser-based remote sensing techniques for monitoring structural deformation of archeological monuments, J. Archeol. Sci., 40, 176–189, 2013.

Tappin, D. R., Watts, P., McMurtry, G. M., Lafoy, Y., and Matsumoto, T.: The Sissano, Papua New Guinea tsunami of July 1998 – Offshore evidence on the source mechanism, Mar. Geol., 175, 1–23, 2001.

Tarchi, D., Casagli, N., Fanti, R., Leva, D., Luzi, G., Pasuto, A., Pieraccini, M., and Silvano, M.: Landside Monitoring by Using Ground-Based SAR Interferometry: an example of application to the Tessina landslide in Italy, Engin. Geol., 68, 15–30, 2003.

Teza, G., Marcato, G., Castelli, E., and Galgaro, A.: IRTROCK: A MATLAB toolbox for contactless recognition of surface and shallow weakness of a rock cliff by infrared thermography, Computers & Geosciences, 45, 109–118, 2012.

Tinti, S., Maramai, A., and Graziani, L.: The new catalogue of Italian tsunamis, Natural Hazards, 33, 439–465, 2004.

Travelletti, J., Oppikofer, T., Delacourt, C., Malet, J. P., and Jaboyedoff, M.: The International Archives of the Photogrammetry, Remote Sensing and Spatial Information Sciences. Vol. XXXVII, Part B5, Beijing, 2008.

Violante, C.: Geohazard in Rocky Coastal Areas, Geological Society, London, Special, Publications, 322 pp., 2009.

Vlcko, J., Greif, V., Grof, V., Jezny, M., Petro, L., and Brcek, M.: Rock displacement and thermal expansion study at historic heritage sites in Slovakia, Environ. Geol., 58, 1727–1740, 2009

Wust-Block, H. G.: Characterizing and locating very weak ($-2.2 \geq M_L \geq -3.4$) induced seismicity in unstable sandstone cliffs by nanoseismic monitoring, Pure Appl. Geophys., 167, 153–167, 2010.

Yang, X., Stump, B. W., and Phillips, W. S.: Source Mechanism of an Explosively Induced Mine Collapse, Bull. Seismol. Soc. Am., 88, 843–854, 1998.

Zhang, J., Tang, W. H., and Zhang, L. M.: Efficient probabilistic back-analysis of slope stability model parameters., J. Geotechn. Geoenviron. Engin., 136, 99–109, 2010.